

Cross sections for L -subshell ionization in Au by the collision of protons and helium ions*

S. Datz

Oak Ridge National Laboratory, Oak Ridge, Tennessee 37830[†]

J. L. Duggan

Oak Ridge Associated Universities, Oak Ridge, Tennessee 37830[†]

L. C. Feldman

Bell Telephone Laboratories, Murray Hill, New Jersey 07974
Physics Institute, University of Aarhus, Aarhus, Denmark

E. Laegsgaard and J. U. Andersen

Physics Institute, University of Aarhus, Aarhus, Denmark
(Received 23 July 1973)

Absolute ionization cross sections for the L subshells of Au by proton bombardment (0.25–5.2 MeV) have been determined from data obtained using a Si(Li) detector and the presently available values for radiative transition probabilities, fluorescence yields, and Coster-Kronig factors. The measured cross sections are compared with values calculated by Choi using the plane-wave Born approximation (PWBA) with either relativistic or nonrelativistic hydrogenic wave functions for the Au electrons. Except at low energies ($\eta_L/\theta_L^2 < 0.2$) where the uncorrected PWBA is questionable, the agreement is good. A plateau in the $2s$ ionization cross section attributable to the bimodal $2s$ -electron wave function is observed in the region 0.5–1.0 MeV. Ionization by He ions (1–12 MeV) is similar, but significant differences in subshell behavior are observed.

Considerable effort in recent years has gone into the theoretical and experimental determination of inner-shell ionization by heavy-ion bombardment.¹ The case of K -shell ionization has been extensively investigated, and agreement between theory and experiment for simple projectiles (i.e., protons and helium ions) is remarkably good. Similarly, total ionization cross sections for L -shell electrons are in fair accord with predictions. Separate contributions of L subshells have been calculated but have not been well established experimentally. Of particular interest is the energy dependence of the $2s_{1/2}$ ionization. Here we have the first case of an orbital with a radial node. Insofar as the plane-wave Born approximation (PWBA) can be viewed as predicting an increasing effective impact parameter for ionization with increasing energy, a nonmonotonic increase in the ionization cross section might be expected. Subshell ionization cross sections for Au have been calculated by Choi using both relativistic² and nonrelativistic³ hydrogenic wave functions for the L electrons. These have been partially tested by Bissinger *et al.*,⁴ who compared the intensity ratios of gross spectral features ($L\alpha$, $L\beta$, $L\gamma$) with the predictions of Choi, but neither the absolute subshell cross sections nor the subshell cross-section ratios were adduced.

In this work we have measured Au L x-ray spectra induced by proton (0.25–5.2 MeV) and helium-

ion (1–12 MeV) bombardment in thin (100- $\mu\text{g}/\text{cm}^2$) Au targets using Oak Ridge Van de Graaff accelerators and a Si(Li) detector (resolution: 175 eV). A typical spectrum is shown in Fig. 1. The spectrum anticipated assuming equal probability of $2s_{1/2}$, $2p_{1/2}$, and $2p_{3/2}$ ionization is shown in Fig. 2. (Except as noted, the radiative transition probabilities used in this work are taken from the calculations of Scofield,⁵ and the fluorescence yield and Coster-Kronig factors used are those of McGuire.⁶)

With the resolution attainable, the Au L x-ray spectrum can be subdivided into three main portions: the $\alpha_{1,2}$ group, which arises from $2p_{3/2}$ vacancy filling; the β group, which contains unresolved contributions from all three subshells; and the γ group (Fig. 3), which contains contribu-

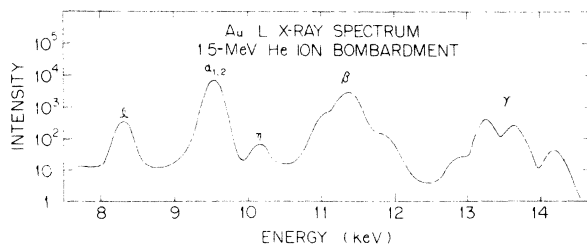


FIG. 1. Au L x-ray spectrum recorded with a 175-eV-resolution Si(Li) detector.

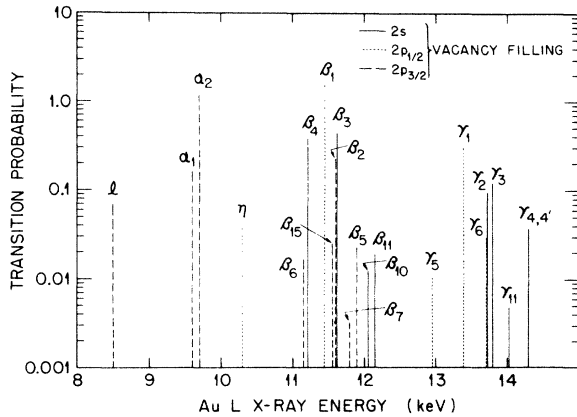


FIG. 2. Radiative transition probabilities for lines in the Au *L* x-ray spectrum. The solid lines, dotted lines, and dashed lines correspond to transitions in which vacancies in $2s_{1/2}$, $2p_{1/2}$, and $2p_{3/2}$ levels, respectively, are filled. Transition probabilities are taken from the calculation of Scofield (Ref. 5).

tions from $2p_{1/2}$ (γ_1 , γ_5 , and γ_6) and $2s$ ($\gamma_{2,3}$, $\gamma_{4,4'}$). The γ_6 and $\gamma_{2,3}$ lines are unresolvable, but, if the transition probability ratio $\tau_{\gamma_6}/\tau_{\gamma_1}$ is known, the γ_6 contribution to the intensity can be subtracted from the area $A(\gamma_{2,3} + \gamma_6)$ complex. This ratio was

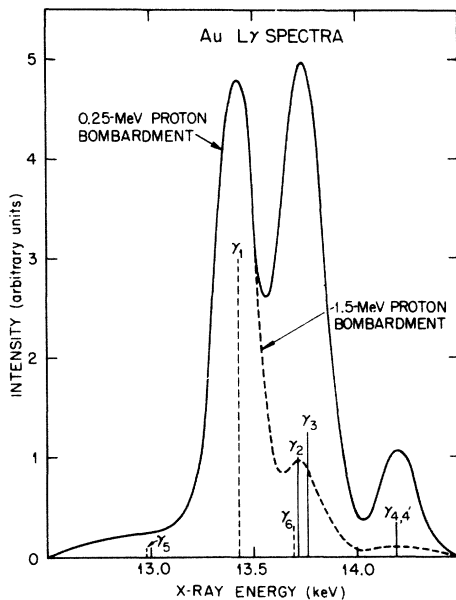


FIG. 3. Variations in the γ portion of Au *L* x-ray spectra observed by bombardment with protons at 1.5 MeV (dotted curve) and 0.25 MeV (solid curve). The vertical lines indicate the positions of the anticipated x-ray lines (dashed lines originate from $2p_{1/2}$ vacancies and solid lines from $2s_{1/2}$ vacancies). The heights of the lines are proportional to the transition probabilities calculated by Scofield (Ref. 5).

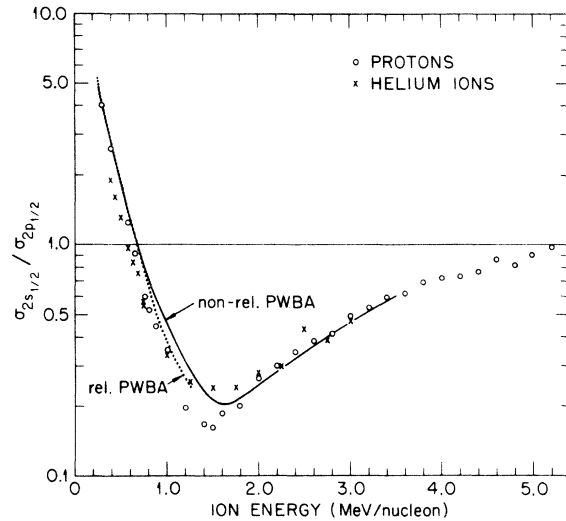


FIG. 4. Ratio of $2s_{1/2}$ to $2p_{1/2}$ ionization cross section in Au for protons (0.25–5.2 MeV) and He ions (1–12 MeV) compared with relativistic PWBA and nonrelativistic PWBA calculations of Choi (Refs. 2 and 3).

determined by Cooper⁷ to be 0.11 and calculated by Scofield⁵ to be 0.094. Since the ratio of the intensities in the γ group varies significantly with energy (Fig. 3), an independent determination of the relative transition probabilities $\tau_{\gamma_6}/\tau_{\gamma_1}$ could be made, i.e.,

$$A(\gamma_{2,3} + \gamma_6) = (\tau_{\gamma_6}/\tau_{\gamma_1})A(\gamma_1) + (\tau_{\gamma_{2,3}}/\tau_{\gamma_{4,4'}})A(\gamma_{4,4'}).$$

A plot of $A(\gamma_{2,3} + \gamma_6)/A(\gamma_1)$ versus $A(\gamma_{4,4'})/A(\gamma_1)$ was indeed linear and, from the intercept, $\tau_{\gamma_6}/\tau_{\gamma_1}$ was found to be 0.125 ± 0.01 .

The initial vacancy production in the $2s$ subshell, $V(2s)$, could then be determined from

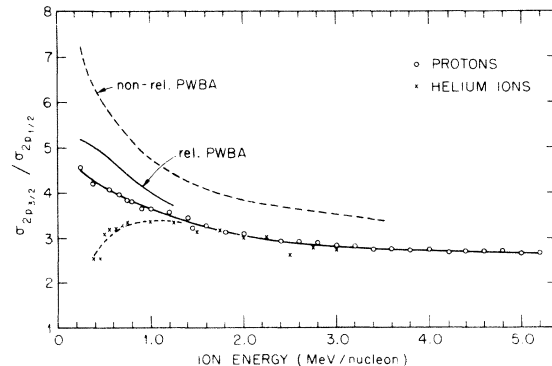


FIG. 5. Ratio of $2p_{3/2}$ to $2p_{1/2}$ ionization cross section in Au for protons (0.25–5.2 MeV) and He ions (1–12 MeV) compared with relativistic PWBA and nonrelativistic PWBA calculations of Choi (Refs. 2 and 3).

$$V(2s) = [\tau_t(2s)/(\tau_{\gamma_{2,3}})(\omega_{2s})] \\ \times [A(\gamma_{2,3} + \gamma_6) - (\tau_{\gamma_6}/\tau_{\gamma_1})A\gamma_1],$$

where τ_t is the radiative transition probability for a given line, $\tau_t(2s)$ is the total radiative transition probability, and ω_{2s} is the 2s fluorescence yield.

The initial vacancy production in the $2p_{1/2}$ subshell could then be obtained from

$$V(2p_{1/2}) = [\tau_t(2p_{1/2})A(\gamma_1)/\tau_{\gamma_1}\omega_{2p_{1/2}}] - f_{1,2}V(2s),$$

where $f_{1,2} = 0.083$ is the Coster-Kronig fraction feeding $2p_{1/2}$ from 2s. Here we used $\tau_{\gamma_1} = 0.33$, which we obtained from the recent determination of Salem *et al.*⁸ for $(\tau_{\gamma_1}/\tau_{\beta_1}) = 0.211$ and the calculated value² for τ_{β_1} .

Finally, for the $2p_{3/2}$ subshell we have

$$V(2p_{3/2}) = [\tau_t(2p_{3/2})A(\alpha_{1,2})/\tau_{\alpha_{1,2}}\omega_{2p_{3/2}}] \\ - f_{1,3}V(2s) - f_{2,3}V(2p_{1/2}),$$

where $f_{1,3} = 0.6444$ and $f_{2,3} = 0.132$ are the Coster-Kronig fractions for feeding $2p_{3/2}$ and $2p_{1/2}$, respectively.

As a check on the consistency of the transition probabilities used, we computed the total area of the unresolved β -complex spectrum from

$$A_{\beta \text{ complex}} = (A_{\alpha_{1,2}}/\tau_{\alpha_{1,2}})(\tau_{\beta_{2,11}} + \tau_{\beta_5} + \tau_{\beta_6}) \\ + A_{\gamma_1}(\tau_{\beta_1}/\tau_{\gamma_1}) + (A_{\gamma_{2,3}}/\tau_{\gamma_{2,3}}) \\ \times (\tau_{\beta_4} + \tau_{\beta_3} + \tau_{\beta_9} + \tau_{\beta_{10}}),$$

using the transition probability ratios given by Salem *et al.*⁸ for the $2p_{3/2}$ and $2p_{1/2}$ factors and the

calculated values of Scofield⁵ for the 2s portion. The average deviation of the calculated β -complex peak area from 17 measured areas was only 2%, with a maximum error of 4%.

The ratio of ionization cross sections for the 2s subshell [$\sigma_I(2s)$] to that for the $2p_{1/2}$ subshell is obtained simply from $V(2s)/V(2p_{1/2}) = \sigma_I(2s)/\sigma_I(p_{1/2})$. This ratio is plotted in Fig. 4 versus particle energy in MeV/nucleon for both proton and He-ion projectiles. A similar plot for $\sigma_I(2p_{3/2})/\sigma_I(2p_{1/2})$ is shown in Fig. 5.

Absolute ionization cross sections were determined as follows: The absolute cross section for generation of $\alpha_{1,2}$ x rays, $\sigma^x(\alpha_{1,2})$, was obtained by comparing the number of counts in the $\alpha_{1,2}$ peak to the Rutherford scattering counts on a solid-state detector placed at 90° to the beam direction. The efficiency of the x-ray detector was calibrated with standard x-ray sources obtained from the National Bureau of Standards and the International Atomic Energy Agency. The solid angle subtended by the Rutherford detector was determined with a calibrated ²⁴⁴Cm α source made by the Transuranium Research Laboratory at Oak Ridge National Laboratory. The vacancy production cross section in $2p_{3/2}$ is given by

$$\sigma_v(2p_{3/2}) = (\sigma_{\alpha_{1,2}}^x/\omega_{2p_{3/2}})[\tau_t(p_{3/2})/\tau_{\alpha_{1,2}}] \\ = \sigma_I(2p_{3/2}) + f_{2,3}\sigma_I(2p_{1/2}) + f_{1,3}\sigma_I(2s).$$

Using the above-determined values of the subshell cross section ratios the absolute ionization cross sections are determined, e.g.,

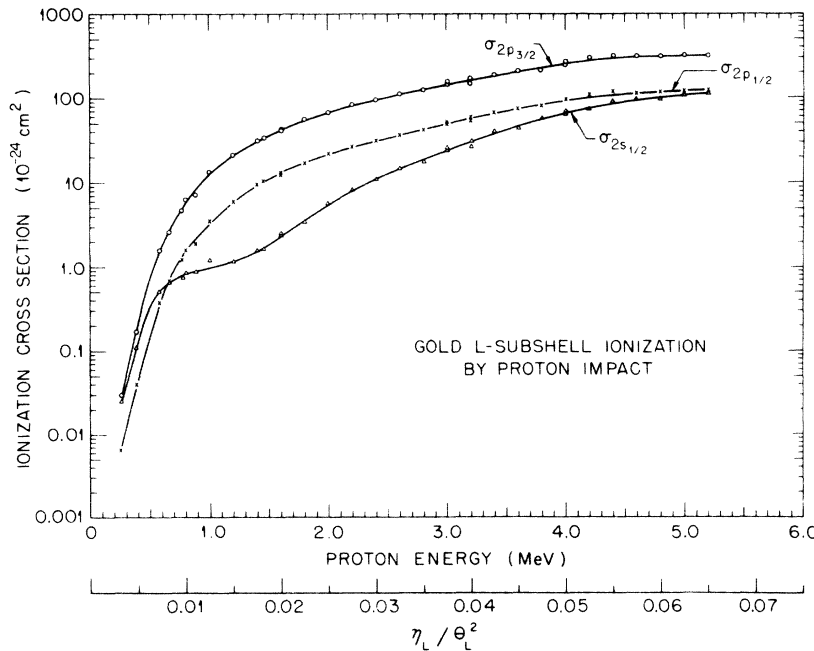


FIG. 6. Absolute ionization cross sections for Au L subshells as a function of proton energy in MeV and in reduced units (η_L/θ_L^2).

$$\sigma_I(2p_{1/2}) = \sigma_v(2p_{3/2}) / \{f_{L,3} [\sigma_I(2s) / \sigma_I(2p_{1/2})] + [\sigma_I(2p_{3/2}) / \sigma_I(2p_{1/2})] + f_{2,3}\}.$$

These cross sections are plotted in Fig. 6 as a function of energy. The energy units are given both in MeV and the reduced energy units⁹ η_L/θ_L^2 . Here $\eta_L = mE/MZ_L^2R_\infty$ and the screening parameter $\theta_L = 4I_{2s}/Z_L^2R_\infty$, where $Z_L = Z - 4.15$ is the effective Z of the nucleus corrected for screening by inner-shell electrons and I_{2s} is the binding energy of the $2s$ electron (14.3 keV for Au). For the proton-Au system $\eta_L/\theta_L^2 = 0.0126E$ (in MeV).

The plateau in the $2s_{1/2}$ ionization cross section (Fig. 6) has been anticipated by Merzbacher⁹ and Hansteen and Mosebekk.¹⁰ It can be understood either in terms of the bound-electron momentum wave function or the corresponding configuration-space wave function. As Merzbacher shows, the cross section at low energies is proportional to the square of the magnitude of the momentum wave function. The $2s_{1/2}$ -state momentum wave function has a zero at a momentum of $Z_L\hbar/2a_0$, and a corresponding change in the energy dependence of the cross section is predicted^{2,3} at $\eta_L/\theta_L^2 \approx 0.01$ (0.8 MeV). This is clearly apparent in the data shown in Fig. 6.

Perhaps a more descriptive picture is provided by the semiclassical analysis (SCA) of Hansteen and Mosebekk.¹⁰ In this analysis one may think of only impact parameters less than $\hbar v/I_i$ contributing to the ionization cross section. The electron density profiles shown in Fig. 7 indicate that at low energies, where small impact parameters dominate, the projectile interacts primarily with the $2s_{1/2}$ electron.

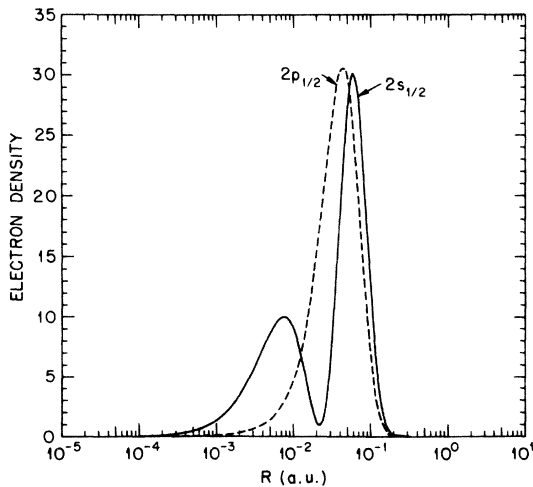


FIG. 7. Radial distribution of electron densities $(\psi_r/r)^2$ for $2s_{1/2}$ and $2p_{1/2}$ electrons in Au calculated with relativistic Hartree-Fock-Slater wave functions [T. A. Carlson (unpublished)].

As the energy and relevant impact parameter increase, the relevant portion of the $2s_{1/2}$ density profile goes through a node, while the relevant portion of $2p_{1/2}$ density increases monotonically—implying a different energy dependence for the ionization of these two subshells.

A comparison with the absolute PWBA cross sections calculated by Choi is shown in Fig. 8. The calculations, using nonrelativistic hydrogenic wave functions, agree very well with the data at energies greater than 1 MeV. Below 1 MeV the data drop below the calculated curve and at 0.25 MeV are a factor of ~ 4 lower than the nonrelativistic calculation and a factor of ~ 10 lower than the PWBA utilizing relativistic wave functions. Although the use of hydrogenic wave functions may partially contribute to the discrepancy, this departure probably reflects the inadequacy of the PWBA at low velocities for the high- Z target used. The effects of hyperbolic paths¹¹ and binding¹² tend to decrease the cross section at low velocities, and calculations on these effects for this system are presently underway.¹³ Since these effects should affect all of the partial cross sections in a similar manner, a comparison of cross section ratios might be instructive. In Fig. 4 the $\sigma_{2s_{1/2}}/\sigma_{2p_{1/2}}$ ratio is shown to match the predictions of the relativistic PWBA exceedingly well in the range

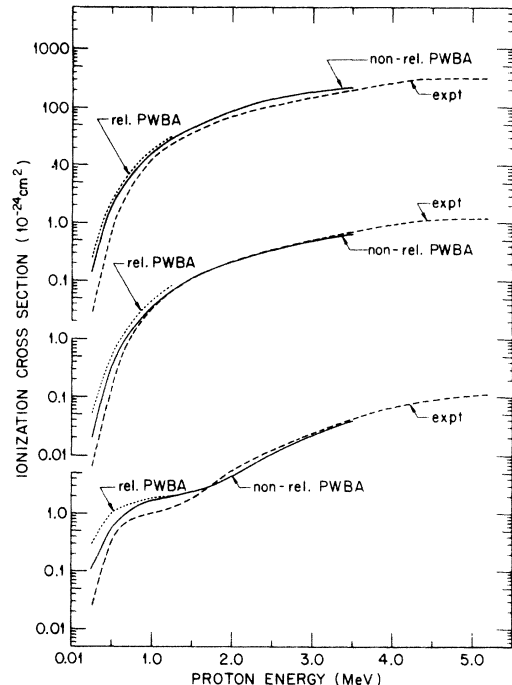


FIG. 8. Comparison of calculated L subshell ionization cross sections using relativistic and nonrelativistic electron wave functions with experimental results.

covered in the calculations, and to fit very well with the nonrelativistic PWBA at higher velocities. Again, in Fig. 5, the $\sigma_{2p_{3/2}}/\sigma_{2p_{1/2}}$ ratio is a somewhat better fitted by the calculations using relativistic wave functions.

The He-ion data shown in Figs. 4 and 5 show significant deviations from the proton data at low energies. Especially puzzling is the downward trend in $\sigma_{2p_{3/2}}/\sigma_{2p_{1/2}}$ at below 1.5 MeV/nucleon. At this point it is well to recall that the ionization cross sections deduced from the data and presented here are based upon the validity of a set of radiative transition probabilities, fluorescence yields, and Coster-Kronig fractions, which can be affected by

multiple excitation of the target atom. In particular, in this analysis $\sigma_I(2p_{1/2})$ is deduced from transitions which involve electrons in the *N* and *O* shells, whereas $\sigma_I(2p_{3/2})$ is determined primarily by transitions involving electrons in the *M* shell. Evidence for a greater degree of multiple ionization by low-energy He ions *vis à vis* protons has been shown,¹⁴ and the apparent cross-section effects may be due to these differences.

The authors gratefully acknowledge stimulating discussions with Professor E. Merzbacher and thank Dr. B. H. Choi for giving us the results of his calculations prior to publication.

*Paper first presented at the International Conference on Inner Shell Ionization, Atlanta, Ga., April 17–22, 1972.

†Research sponsored by the U. S. Atomic Energy Commission under contract with Union Carbide Corporation.

¹*Proceedings of the International Conference on Inner Shell Ionization Phenomena, Atlanta, Georgia, 1972*, edited by R. W. Fink, S. T. Manson, J. M. Palms, and P. V. Rao (U. S. AEC, Oak Ridge, Tenn., 1973).

²B.-H. Choi (private communication).

³B.-H. Choi, E. Merzbacher, and G. S. Khandelwai, *At. Data* **5**, 291 (1973).

⁴G. A. Bissinger, A. B. Baskin, B.-H. Choi, S. N. Shafroth, J. M. Howard, and A. W. Waltner, *Phys. Rev. A* **6**, 545 (1972); S. N. Shafroth, G. A. Bissinger, and

A. W. Waltner, *Phys. Rev. A* **7**, 566 (1973).

⁵J. H. Scofield, *Phys. Rev.* **179**, 9 (1969).

⁶E. J. McGuire, *Phys. Rev. A* **3**, 587 (1971).

⁷J. N. Cooper, *Phys. Rev.* **61**, 234 (1942).

⁸S. I. Salem, R. T. Tsutsui, and B. A. Rabbani, *Phys. Rev. A* **4**, 1728 (1971).

⁹E. Merzbacher, in Ref. 1, p. 915ff.

¹⁰J. M. Hansteen and O. P. Mosebekk, *Nucl. Phys. A* **201**, 541 (1973).

¹¹J. Bang and J. M. Hansteen, *Mat. Fys. Medd. Vis. Selsk.* **31**, No. 13 (1959).

¹²G. Basbas, W. Brandt, and R. Laubert, *Phys. Rev. A* **7**, 983 (1973).

¹³W. Brandt and G. Lapiki (private communication).

¹⁴A. R. Knudson, P. G. Burkhalter, and D. J. Nagel, in Ref. 1, p. 1675ff.